

Surface Sensing of 3D Objects Using Vibrissa-like Intelligent Tactile Sensors

1st Lukas Merker

Dept. of Mech. Engineering
Technische Universität Ilmenau

Ilmenau, Germany

e-mail: lukas.merker@tu-ilmenau.de

2nd Moritz Scharff

Dept. of Mech. Engineering
Technische Universität Ilmenau

Ilmenau, Germany

3rd Klaus Zimmermann

Dept. of Mech. Engineering
Technische Universität Ilmenau

Ilmenau, Germany

4th Carsten Behn

Dept. of Mech. Engineering
Schmalkalden University of Applied Sciences

Schmalkalden, Germany

e-mail: c.behn@hs-sm.de

Abstract—Interacting with the environment, many robots would benefit from advanced tactile sensors complementing optical sensors in particular when operating under poor visibility. In nature, rats exhibit a prominent tactile sense organ, the so-called vibrissae. For instance, these enable rats to detect shape and texture information of objects based on few contacts. Since vibrissae consist of dead tissue, all sensing is performed in the support of each vibrissa, the follicle-sinus complex. Inspired by this characteristic measuring principle, we set up a mechanical model, consisting of a cylindrical, one-sided clamped bending rod, which is swept along a 3D object surface undergoing large deflections. In doing so, the focus is on both simulating the scanning sweep in order to determine the support reactions of the rod during object scanning and subsequently using these quantities in order to reconstruct a sequence of contact points as a basis for shape reconstruction. The simulated scanning sweeps include tip and tangential contacts, as well as longitudinal, lateral and axial slip. The object reconstruction reveals that simple scanning kinematics, e.g., passive dragging of the tactile sensor on a mobile robot, are sufficient in order to capture fragments of object shapes and thus to complement data gathered by optical sensors.

Keywords—Vibrissa; tactile sensor; surface sensing; surface reconstruction;

I. INTRODUCTION

A prominent and particularly well researched sense organ are the mystacial vibrissae in the snout region of the rat, enabling the animals to gather information about object distances, orientations, shapes and textures, as well as fluid flows [1]–[4]. Basically, a vibrissa consists of a long and slender hair-shaft with no receptors along its length, which is conical and pre-curved [5][6] and supported by the Follicle Sinus Complex (FSC) [7][8]. Making contact with an object of interest, mechanical stimuli are transmitted through the hair-shaft to the FSC, where the actual sensing is realized by a wide variety of mechanoreceptors, which are radially and longitudinally distributed along the follicle [9]. Despite the fact that it is not conclusively clarified how exactly animals manage to determine object features, e.g., object shapes [10], the basic measuring principle of a vibrissa often serves as a paragon for developing tactile sensors.

In literature, a large number of vibrissa-inspired sensor principles with a focus on object scanning and reconstruction

can be found. These approaches differ considerably in the modulation of the vibrissa-shaft and its support, the evaluated signals (observables) and the procedure of localizing contact points, as a basis for shape reconstruction. Usually, the focus is on the actual object reconstruction based on different measured signals at the base of a rod-shaped structure. However, a theoretical generation of the support reactions during object scanning is rarely taken into account. For the process of object scanning, two different approaches have been established in literature [11]: Firstly, an object can be scanned using a tapping strategy, i.e., tapping the artificial vibrissa against various points of the objects surface by small pushing angles. In doing so, the artificial vibrissa is retracted from the object right after the very first contact resulting in only small deformations of the artificial vibrissa. Therefore, many approaches use linear bending theory to accomplish the localization of the contact points [12]–[15]. For that purpose, curvature or torque information at the base of the artificial vibrissa [15] or even its base angles and/or moments [12]–[14] are evaluated. Secondly, there is the sweeping strategy. In this case, the rod is pushed against an object far beyond the very first contact, consequently undergoing large deformations and sliding over the object's surface. Therefore, a highly flexible and elastic artificial vibrissa must be used. In [11], a sweeping reconstruction algorithm was presented, which is based on repeatedly inferring from one contact point to the next one by continuous measurement of the moment and rotation angle at the base of the rod. This method dispenses the need of force measurements, but it is limited to tangential contacts along the artificial vibrissa and cannot be used for 3D reconstruction. Another reconstruction approach using the sweeping scanning strategy and evaluating moments and forces at the base of a rod was used in [16] and [17]. In [17], the focus was on the mechanical model, which was limited to a plane and treated analytically. In doing so, the support reactions were generated analytically in a first step, validated using an experimental setup and used for object reconstruction in a second step. With the goal of 3D object scanning, the authors in [16] used a hub load cell to measure the support reactions at the base of a steel wire, which was swept along several edged 3D objects. During scanning, lateral slip of the artificial vibrissa was prevented by adjusting the scanning direction based on the surface normal, which was determined exploiting the support reactions. In

contrast to [17], the support reactions were only measured but not generated theoretically. In [18], the authors modeled an artificial vibrissa using a multi-body system. There, the step of generating the support reactions in 3D space was included, but only for an a priori known external load. In addition, the applied force was always perpendicular to the artificial vibrissa, although contact forces at the tip of an artificial vibrissa may have arbitrary orientations in many real world scenarios. The model presented within this paper differs from [18] by considering a changing contact force resulting from the sweep of a rod along a mathematically described object surface. Adapting the model of [17] for 3D scanning and reconstruction, we focus on both, shape reconstruction of 3D objects with a wide-ranging curvature (in contrast to [16]) **and** a theoretically generation of the support reactions during object scanning. The latter provides an important basis for future parameter studies without the necessity of performing a large amount of experiments. During object scanning, tip and tangential contacts are taken into account. Objects are scanned on a straight trail without actively adjusting the scanning direction in order to prevent lateral slip.

The paper at hand is structured in the following way: In Section II the mechanical sensor model is presented and used in two steps: Firstly, we demonstrate, how the support reactions at the base of the sensor during a scanning sweep along a prescribed 3D object surface can be generated theoretically. Secondly, we present a procedure of reconstructing a sequence of contact points solely based on the support reactions, which might either be known from the previous step or by measurements. Both steps are implemented in a scanning and reconstruction algorithm. In Section III this algorithm is used for simulating scanning sweeps along an exemplary 3D surface, analyzing the support reactions at the base of the sensor. Afterwards, these signals are used in order to reconstruct multiple points on the object's surface. Finally, the results of the present paper are summed up and some future research subjects are identified in Section IV.

II. MODELLING

The mechanical model consists of a one-sided clamped rod (highly elastic probe) and an object in a fixed Cartesian (x, y, z) -coordinate system, see Figure 1. The rod is circular-cylindrically shaped and therefore characterized by the length L and a constant circular cross-section, resulting in a constant second moment of area I . It consists of a homogeneous and isotropic material with a constant Young's modulus E . From the outset, we introduce the following units of measure using the mentioned parameters of the rod in order to allow any kind of scaling [17]:

$$\begin{aligned} [\text{length}] &:= L, \\ [\text{force}] &:= EI/L^2, \\ [\text{moment}] &:= EI/L \end{aligned} \quad (1)$$

The object is assumed as a rigid body with a strictly convex, smooth surface $z = C(x, y)$. The scanning sweep of the rod along the object's surface is realized by a kinematic drive, in a way that the clamping position $P_0(x_0, y_0, 0)$ of the rod (system input) is shifted incrementally along a straight trail in the x - y -plane.

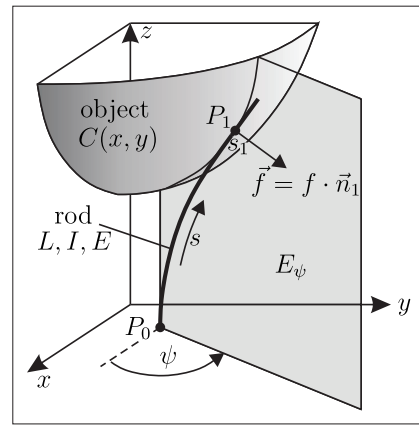


Figure 1. Model for object shape scanning and reconstruction – rod in contact with an object's surface.

After the very first contact between the undeformed rod and the object, the rod gets bent and slides along the surface, see Figure 1. This process is treated as a quasi-static one. As a consequence of the strict convexity of the object multi-point contacts between the object and the rod are excluded. Thus, each preset clamping position P_0 results in a single contact point $P_1(\xi, \eta, \theta)$ on the surface with some contact force \vec{f} acting on the rod. Neglecting frictional effects (approximation for low-friction material pairings), the contact force \vec{f} with magnitude f coincides with the outward pointing unit normal vector \vec{n}_1 of the surface, see Figure 1:

$$\vec{n}_1 = \frac{\vec{n}_0}{\|\vec{n}_0\|_2}, \quad \text{with} \quad \vec{n}_0 = \begin{pmatrix} -C_{,x}(\xi, \eta) \\ -C_{,y}(\xi, \eta) \\ 1 \end{pmatrix} \quad (2)$$

$$\vec{f} = f \cdot \vec{n}_1 \quad (3)$$

Due to the homogeneity and isotropy of the rod and its support and the single force assumption the elastic line of the rod shrinks to one in a plane E_ψ with some unknown orientation angle ψ (see Figure 1) and the normal vector:

$$\vec{e}_\psi = \begin{pmatrix} -\sin(\psi) \\ \cos(\psi) \\ 0 \end{pmatrix} \quad (4)$$

Thus, parameterizing the elastic line of the rod by means of its slope angle $\varphi(s)$ in dependence on its natural coordinate arc length s yields:

$$\vec{q}(s) = \begin{pmatrix} \frac{dx(s)}{ds} \\ \frac{dy(s)}{ds} \\ \frac{dz(s)}{ds} \end{pmatrix} = \begin{pmatrix} \cos(\varphi(s)) \cos(\psi) \\ \cos(\varphi(s)) \sin(\psi) \\ \sin(\varphi(s)) \end{pmatrix} \quad (5)$$

$$\frac{d\varphi}{ds} = \kappa(s) \quad (6)$$

Using a dimensionless representation of Euler's constitutive law (mind (1)) the curvature $\kappa(s)$ writes

$$\kappa(s) = m(s) = -f \cdot \det(\vec{r}, \vec{n}_1, \vec{e}_\psi) \quad (7)$$

where $m(s)$ is the bending moment with respect to the deformation plane E_ψ and

$$\vec{r} = \begin{pmatrix} \xi - x(s) \\ \eta - y(s) \\ \theta - z(s) \end{pmatrix}. \quad (8)$$

Using (5), the derivative of (7) writes:

$$\kappa'(s) = m(s) = f \cdot \det(\vec{q}(s), \vec{n}_1, \vec{e}_\psi) \quad (9)$$

Together with (5), (6) and (9) we find the following system of Ordinary Differential Equations (ODE) of first order, describing the deformation of the rod in space.

$$\begin{cases} x'(s) = \cos(\varphi(s)) \cos(\psi) \\ y'(s) = \cos(\varphi(s)) \sin(\psi) \\ z'(s) = \sin(\varphi(s)) \\ \varphi'(s) = \kappa(s) \\ \kappa'(s) = f \cdot \det(\vec{q}(s), \vec{n}_1, \vec{e}_\psi) \end{cases} \quad (10)$$

In contrast to the ODE system used in [17], the additional parameter ψ allows the deformation plane to rotate in space (with respect to the z -axis) as a consequence of lateral slip during object scanning. Thus, sweeping the rod along an object on a straight scanning trail, the path of the contact point over the object's 3D surface is not a priori known, as it is the case when scanning 2D object contours. Therefore, the procedure suggested in [17], to determine the rod's base position assuming a given contact point on the object is not appropriate for 3D surface scanning, because the base position corresponding to an arbitrarily preset contact point on the 3D surface would not necessarily lie on the specified scanning trail. Therefore, we proceed in inverse direction using the base position P_0 as system input as a basis for determining the corresponding contact position, what better reflects the practical process.

A. Generating the support reactions theoretically

The boundary conditions are formulated distinguishing between tip contacts and tangential contacts. For tip contacts the contact position s_1 along the rod is known: $s_1 = 1$. For tangential contacts s_1 is unknown but the condition $\vec{q}(s_1) \perp \vec{n}_1 \Leftrightarrow \vec{q}(s_1) \cdot \vec{n}_1 = 0$ must be fulfilled. This results in the following Boundary Conditions (BCs) for tip and tangential contacts, respectively:

$$\text{tip:} \quad \begin{cases} x(0) = x_0 & x(1) = \xi \\ y(0) = y_0 & y(1) = \eta \\ z(0) = 0 & z(1) = \theta \\ \varphi(0) = \frac{\pi}{2} & \\ & \kappa(1) = 0 \end{cases} \quad (11)$$

$$\text{tangential:} \quad \begin{cases} x(0) = x_0 & x(s_1) = \xi \\ y(0) = y_0 & y(s_1) = \eta \\ z(0) = 0 & z(s_1) = \theta \\ \varphi(0) = \frac{\pi}{2} & \vec{q}(s_1) \cdot \vec{n}_1 = 0 \\ & \kappa(s_1) = 0 \end{cases} \quad (12)$$

For each clamping position P_0 (system input) on the scanning trail, the Boundary-Value Problems (BVPs) (10)&(11), as well as (10)&(12) are solved (respecting the additional constraint $\vec{n}_1 \cdot \vec{e}_\psi = 0$) using a *Matlab*-algorithm. In doing so, the unknown parameters f , s_1 , ψ , ξ and η are determined using shooting methods. The algorithm proceeds by pre-supposing tip contact, checking s_1 for contradictions (e.g. $s_1 > 1$) afterwards in order to decide which of the BCs (11) and (12) correctly describes the actual deformation state. Once the mentioned parameters are known, the six support reactions at the base of the rod are calculated in the following way:

$$\vec{f}_0 = \begin{pmatrix} f_{0x} \\ f_{0y} \\ f_{0z} \end{pmatrix} = -\vec{f}, \quad (13)$$

$$\vec{m}_0 = \begin{pmatrix} m_{0x} \\ m_{0y} \\ m_{0z} \end{pmatrix} = - \begin{pmatrix} \xi - x_0 \\ \eta - y_0 \\ \theta \end{pmatrix} \times \vec{f} \quad (14)$$

The presented model as well as the simulation algorithm are revised versions of those in [20]. The changes and improvements relate in particular to a transformation of the used coordinate system and a more general analytical formulation of the BCs (11)&(12).

B. Reconstructing contact points using the support reactions

For object reconstruction, we assume the support reactions (13)&(14) to be known either from simulations or measurements. In contrast to the previous step of generating the support reactions, this allows to determine the magnitude of the contact force f , its direction \vec{n}_1 and the orientation ψ of the bending plane E_ψ in advance:

$$f = \|\vec{f}_0\|_2, \quad \vec{n}_1 = -\frac{\vec{f}_0}{\|\vec{f}_0\|_2}, \quad \psi = \text{atan2}(m_{0x}, -m_{0y}) \quad (15)$$

where *atan2* is the four-quadrant inverse tangent [21]. Having all parameters of the ODE system (10) at hand by use of (15), the initial values follow from the known support position P_0 and \vec{m}_0 :

$$\begin{cases} x(0) = x_0 \\ y(0) = y_0 \\ z(0) = 0 \\ \varphi(0) = \frac{\pi}{2} \\ \kappa(0) = -\vec{m}_0 \cdot \vec{e}_\psi \end{cases} \quad (16)$$

Thus, the step of object reconstruction requires the solution of an Initial-Value Problem (IVP) only. The contact point is localized by integrating (10)&(16) with the termination condition, that the curvature at the contact point is zero ($\kappa(s_1) = 0$).

III. RESULTS & DISCUSSION

For all simulations, we used an elliptic paraboloid as an exemplary object surface:

$$(x, y) \mapsto C(x, y) = 0.5x^2 + y^2 + h \quad (17)$$

with the object distance $h = 0.4$. The scanning sweeps were realized by shifting the clamping position P_0 on a straight scanning trail in negative x -direction with a constant lateral displacement $y_0 = -0.5:0.1:0.5$ from the coordinate origin, resulting in a total of eleven trails in the x - y -plane. In Figure 2, the signal strengths of all support reactions generated as described in Subsection II-A are indicated by the color-bars and plotted against the base positions during object scanning (scanning trails).

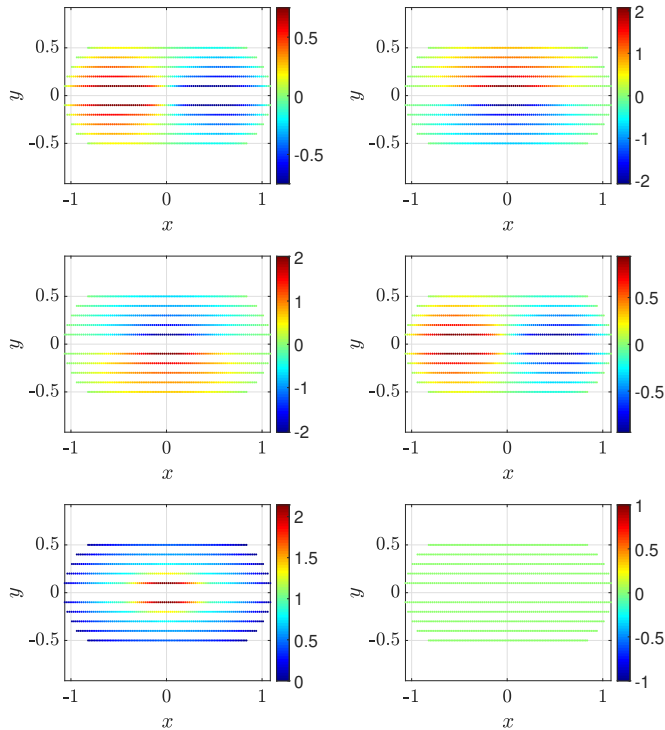


Figure 2. Signal strengths of the observables (support reactions) during object scanning on different scanning trails – reaction forces f_{0x} , f_{0y} and f_{0z} (TB) on the left and reaction moments m_{0x} , m_{0y} and m_{0z} (TB) on the right. The color-bars on the right indicate the signal strengths.

The reaction forces f_{0x} , f_{0y} and f_{0z} from Top to Bottom (TB) are shown on the left and the reaction moments m_{0x} , m_{0y} and m_{0z} (TB) on the right. The color-bars indicate the dimensionless signal strengths for each clamping position (mind (1)). The scanning trail $y_0 = 0$ is omitted in Figure 2 for two reasons: On the one hand, it represents a plane special case with longitudinal slip (contact point movement over the surface within the sensing plane) only, which is not in the focus of the present paper, since it was already analyzed in detail in [17]. On the other hand, the corresponding signals of this sweep are significantly higher compared to all other scanning sweeps and would therefore impair the comparability in Figure 2. It is striking that all components of the support reactions show some symmetric patterns, due to the symmetry of the object. The maximum values of all components increase for smaller values $|y_0|$, i.e., the closer the scanning trail is to the coordinate origin. Mind that all diagrams in Figure 2 have to be read from right to left due to scanning in negative x -direction. It is obvious that the component f_{0x} changes in sign from minus to plus for all chosen scanning trails. The

component f_{0y} is negative for positive values y_0 and vice versa. The vertical component f_{0z} is always positive and a glance on the entirety of all trails already makes it possible to get the idea of some longish convex shape. The clamping moment components behave in a similar way as the reaction forces: The component m_{0x} is positive if $y_0 > 0$ and negative if $y_0 < 0$. The component m_{0y} always changes in sign from minus to plus. A great similarity can be seen between the components f_{0x} and m_{0y} , as well as f_{0y} and m_{0x} . The magnitude of m_{0z} must always be zero, since there is no twist of the rod due to the plane bending assumption. Even though especially the vertical component f_{0z} in Figure 2 might give a rough hint on the scanned object shape, the support reactions do not allow a more precise conclusion about the scanned object shape based on purely visual observation. Therefore, the support reactions from Figure 2 are used for the actual object reconstruction as described in Subsection II-B.

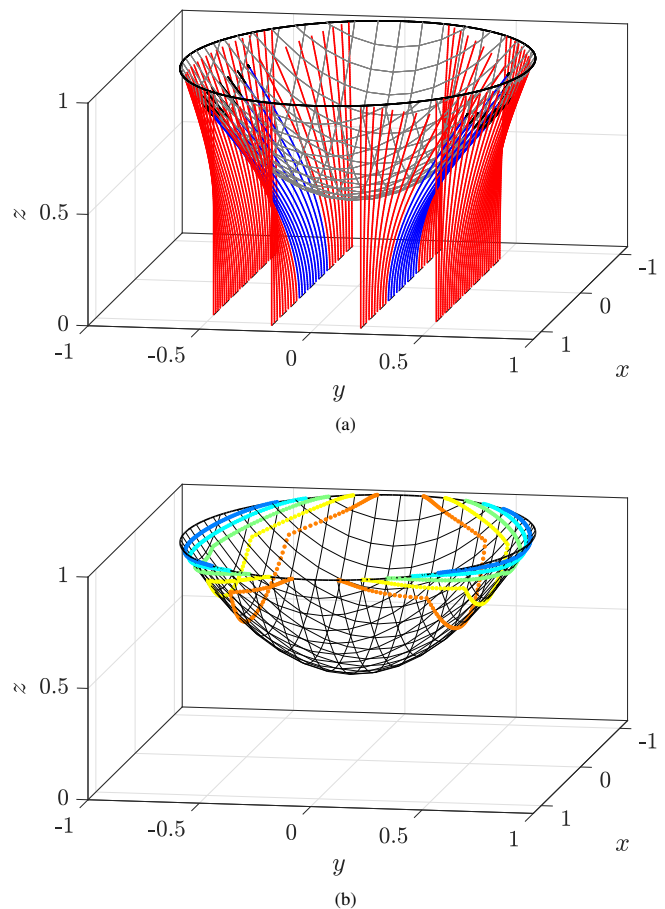


Figure 3. Object surface scanning and reconstruction: (a) Reconstructed elastic lines during object scanning – tip contacts $s \in (0, 1]$ in red, tangential contacts $s \in (0, s_1]$ in blue and $s \in (s_1, 1]$ in black; (b) Reconstructed sequences of contact points based on ten scanning sweeps.

Figure 3a shows the reconstructed elastic lines during sweeps along the elliptic paraboloid (17) on four exemplary scanning trails $y_0 \in \{-0.5; -0.2; +0.2; +0.5\}$. Tip contacts are colored in red. For tangential contacts, the interval $s \in (0, s_1]$ is colored in blue and the straight end $s \in (s_1, 1]$ in black. It can be seen that for each sweep, starting with the

very first contact between the undeformed rod and the surface, the rod bends around the object symmetrically and finally detaches from the object without any snap-off, as observed during plane object scanning [17]. This highlights the fact, that the 2D scanning scenario analyzed in [17] is a special case, which only occurs for special object geometries and arrangements. However, in a real world scanning scenario, geometries and orientations of scanned objects are not known in advance. Therefore, the special case considered in [17] can not be guaranteed and is therefore rather unlikely to occur in reality.

For large lateral displacements $|y_0|$, only tip contacts occur. In contrast, for lower lateral displacements $|y_0|$, tangential contacts increasingly occur. In these cases, the sweep starts with a sequence of tip contacts, continues with tangential contacts and finally ends with another tip contact phase. Of course, for tip contacts ($s_1 = 1$), no axial slip (contact point movement along the rod) but lateral slip (contact point movement along the object's surface) occurs during scanning. For tangential contact, axial and lateral slip occur simultaneously. In Figure 3b the original object surface is superimposed with the reconstructed sequences of contact points. The colors are arbitrary chosen and intended to make it easier to visually distinguish the individual sequences, each resulting from one scanning sweep. The sharp edges in the contact point sequences, in particular evident in the innermost (orange and yellow) sequences result from the transition from tip to tangential contact and vice versa. It is striking that the reconstructed points are unevenly distributed over the scanned surface in a way that especially the lateral area of the surface is characterized by a high density of points. As a consequence, a large reconstruction gap in the area below the center of the object remains. This is due to the fact that even though the trails were distributed equidistantly below the object (see Figure 2), there seems to be an area enclosed by the innermost orange sequences in Figure 3b, which cannot be reached by the rod. However, it can be assumed that the size of this gap might be reduced by scanning in different directions (e.g. perpendicular to the trails in Figure 2) or/and at different object distances h . Returning to the biological paragon, both ideas can be found in the whisking behavior of rats during object exploration [19]. Besides the reconstructed contact points in Figure 3b, the presented measuring principle provides the surface normals at each point, evaluating (15). Thus, the sensed data consisting of a 3D point cloud accompanied by normal vectors is very similar to the one provided by some optical systems, e.g., a laser range finder. This highlights that the presented measuring principle is highly suitable to complement optical sensors in robot exploration and path planning tasks.

IV. CONCLUSION

Within the paper at hand we presented a vibrissa-inspired tactile measuring principle for 3D object surface scanning and reconstruction. In doing so, we considered two consecutive processes separately: firstly, we analyzed the process of theoretically generating the support reactions at the base of a rod, which is swept along a 3D object surface. Secondly, we demonstrated how to use these quantities in order to reconstruct sequences of contact points on the object's surface. Both steps were implemented in an algorithm and simulated to demonstrate the general applicability. Instead of representing a

self-contained investigation, the present paper should be seen as a preliminary concept study. However, it demonstrates that the presented measuring principle is well suited to complement optical sensors in the environmental exploration of robots. By clarifying which mechanical signal strengths are detected during object scanning and how these signals can be used for object reconstruction, we provided a basis for further investigations connecting the mechanical signals (observables) with the actual measurand (3D surface). In doing so, we aim to implement the presented concept into an intelligent tactile sensor in the future. The findings of the present paper are to be validated using an experimental setup in future works. In this context, the effect of some aspects, which are neglected within the presented paper (in particular friction and dynamical effects) on the reconstruction quality should be examined. In addition, the influence of some external disturbance factors, e.g., temperature variations and wind flows, have to be investigated. First experimental investigations identifying fluid flows were already presented in [22]. As the presented measuring principle can be realized with different materials and sensors, it can be assumed, that the temperature dependence of the overall system determines by the thermal properties of the used materials and force-torque-sensors.

REFERENCES

- [1] M. Brecht, B. Preilowski, and M. M. Merzenich, "Functional architecture of the mystacial vibrissae," *Behav. Brain Res.*, vol. 84, pp. 8197, 1997.
- [2] E. Guić-Robles, C. Valdivieso, and G. Guajardo, "Rats can learn a roughness discrimination using only their vibrissal system," *Behav. Brain Res.*, vol. 31, pp. 285–289, 1989.
- [3] G. E. Carvell and D. J. Simons, "Biometric Analyses of Vibrissal Tactile Discrimination in the Rat," *J. Neurosci.*, vol. 10, pp. 26382648, 1990.
- [4] T. J. Prescott, B. Mitchinson, and R. A. Grant, "Vibrissal behavior and function" *Scholarpedia* 6(10):6642, 2011.
- [5] H. M. Belli, A. E. T. Yang, C. S. Bresee, and M. J. Z. Hartmann, "Variations in vibrissal geometry across the rat mystacial pad: Base diameter, medulla, and taper," *J. Neurophysiol.*, vol. 117, pp. 1807–1820, 2016.
- [6] D. Voges et al., "Structural Characterization of the Whisker System of the Rat," *J. Sens.*, vol. 12, pp. 332–229, 2012.
- [7] D. Campagner, M. H. Evans, M. S. E. Loft, and R. S. Petersen, "What the whiskers tell the brain," *Neurosci.* vol. 368, pp. 95–108, 2018.
- [8] S. Ebara, T. Furuta, and K. Kumamoto, "Vibrissal mechanoreceptors". *Scholarpedia*. 12, pp. 32372. DOI: 10.4249/scholarpedia.32372, 2017.
- [9] T. Furuta et al., "The cellular and mechanical basis for response characteristics of identified primary afferents in the rat vibrissal system," *Curr. Biol.*, vol. 30, pp. 814–826, 2020.
- [10] J. H. Solomon and M. J. Z. Hartmann, "Radial distance determination in the rat vibrissal system and the effects of Weber's law," *Phil. Trans. R. Soc. B.*, vol. 366, pp. 3049–3057., 2011.
- [11] J. H. Solomon and M. J. Z. Hartmann, "Extracting object contours with the sweep of a robotic whisker using torque information," *Int. J. Robot Res.* vol. 29, pp. 1233-1245, 2010.
- [12] J. H. Solomon and M. J. Z. Hartmann, "Artificial whiskers suitable for array implementation: accounting for lateral slip and surface friction," *IEEE Trans. Robot.*, vol. 24, pp. 1157–1167, 2008.
- [13] D. Kim and R. Mller, "Biomimetic whiskers for shape recognition." In *Proceedings of the 1995 IEEE International Conference on Robotics and Automation*, Nagoya, Japan, 21-27 May 1995, pp. 1113-1119.
- [14] M. Kaneko, N. Kanayama, and T. Tsuji, "Active antenna for contact sensing," *IEEE Trans. Robot. Autom.*, vol. 14, pp. 278-291, 1998.
- [15] A. E. Schultz, J. H. Solomon, M. A. Peshkin, and M. J. Z. Hartmann, "Multifunctional Whisker Arrays for Distance Detection, Terrain Mapping, and Object Feature Extraction," *IEEE International Conference*

- on Robotics and Automation, Barcelona, Spain, 18-22 April 2005, pp. 2588-2593.
- [16] T. N. Clements and C. D. Rahn, "Three-Dimensional Contact Imaging With an Actuated Whisker," *IEEE Trans. Rob.*, vol. 22, pp. 844–848, 2006.
- [17] C. Will, C. Behn, and J. Steigenberger, "Object contour scanning using elastically supported technical vibrissae," *ZAMM J. Appl. Math. Mec.*, vol. 98, pp. 289-305, 2018.
- [18] L. A. Huet, J. W. Rudnicki, and M. J. Z. Hartmann, "Tactile sensing with whiskers of various shapes: determining the three-dimensional location of object contact Based on mechanical signals at the whisker base." *Soft Robot.*, vol. 4, pp. 88–103, 2017.
- [19] R. A. Grant, B. Mitchinson, C. W. Fox, and T. J. Prescott, "Active Touch Sensing in the Rat: Anticipatory and Regulatory Control of Whisker Movements During Surface Exploration," *J. Neurophysiol.*, vol. 101, pp. 862-874, 2008.
- [20] L. Merker, J. Steigenberger, and C. Behn, "3D Recognition Of Obstacles Using A Vibrissa-like Tactile Sensor," *IEEE International Conference on Flexible and Printable Sensors and Systems (FLEPS)*, Glasgow, United Kingdom, 08-10 July 2019.
- [21] MathWorks®, Support (R2020b), <https://de.mathworks.com/help/matlab/ref/atan2.html>, retrieved: October, 2020.
- [22] M. Scharff et al., "An artificial vibrissa-like sensor for detection of flows," *Sensors*, vol. 19, 2019.